remote sensing

MDPI

Article

Analysis of BDS-3 Real-Time Satellite Clock Offset Estimated in Global and Asia-Pacific and the Corresponding PPP Performances

Hu Wang [1], Pengyuan Li [2,*], Jiexian Wang [2], Hongyang Ma [3], Yangfei Hou [2] and Yingying Ren [2]

[1] Chinese Academy of Surveying and Mapping, Beijing 100036, China
[2] College of Surveying and Geo-Informatics, Tongji University, Shanghai 200092, China
[3] School of Geomatics Science and Technology, Nanjing Tech University, Nanjing 210037, China
* Correspondence: pyli@tongji.edu.cn

Abstract: The quality of satellite clock offset affects the performances of positioning, navigation and timing services, and thus it is essential to the Global Navigation Satellite System (GNSS). This research focuses on the estimation of BeiDou Navigation Satellite System (BDS) real-time precise satellite clock offset by using GNSS stations located in the Global and Asia-Pacific region based on the mixed-difference model. The precision of the estimated BDS clock corrections is then analyzed with the classification of the orbit types, satellite generations, and atomic clock types. The results show that the precision of the BDS clock offset estimated in the Asia-Pacific for Geosynchronous Earth Orbit (GEO), Inclined Geosynchronous Satellite Orbit (IGSO) and Medium Earth Orbit (MEO) satellites are 0.204 ns, 0.077 ns and 0.085 ns, respectively, as compared to those of clock offsets estimated in globally distributed stations. The average precision of the BDS-3 satellites clock offset estimated in global region is 0.074 ns, which is much better than the 0.130 ns of BDS-2. Furthermore, analyzing the characteristics of the corresponding atomic clocks can explain the performance of the estimated satellite clock offset, and the stability and accuracy of various parameters of the Passive Hydrogen Maser (PHM) atomic clocks are better than those of Rubidium (Rb) atomic clocks. In the positioning domain, the real-time clocks estimated in the global/Asia-Pacific have been applied to BDS kinematic Precise Point Positioning (PPP) in different regions. The Root Mean Square (RMS) of positioning results in global real-time kinematic PPP is within 4 cm in the horizontal direction and about 6 cm in the vertical direction. Hence, the BDS real-time clock offset can supply the centimeter-level positioning demand around the world.

Keywords: BeiDou Navigation Satellite System; BDS-3 satellite clock offset; regional solution; atomic clock physical characteristics; precise point positioning

Citation: Wang, H.; Li, P.; Wang, J.; Ma, H.; Hou, Y.; Ren, Y. Analysis of BDS-3 Real-Time Satellite Clock Offset Estimated in Global and Asia-Pacific and the Corresponding PPP Performances. *Remote Sens.* **2022**, *14*, 6206. https://doi.org/10.3390/rs14246206

Academic Editor: Andrzej Stateczny

Received: 30 October 2022
Accepted: 6 December 2022
Published: 7 December 2022

1. Introduction

With the establishment of the Global Positioning System (GPS), Global Navigation Satellite Systems (GNSS) have developed significantly. Currently, the systems with full constellations in-orbit include GPS, the BeiDou Navigation Satellite System (BDS), and the GLObal NAvigation Satellite System (GLONASS). The Galileo Satellite Navigation System (GALILEO) is at the stage of the global networking construction [1–3]. The construction of BDS in China is divided into three phases, i.e., the BDS-1 system, with a total of two Geosynchronous Earth Orbit (GEO) satellites, was completed in 2000; in 2012, the BDS-2 system, including five GEO satellites, five Inclined Geosynchronous Satellite Orbit (IGSO) satellites, and five Medium Earth Orbit (MEO) satellites, was completed to provide users with positioning, timing, speed measurement and short message communication in the Asia-Pacific; the BDS-3 system, including three GEO satellites, three IGSO satellites, and 24 MEO satellites, was built in 2020, and can provide global users with higher-precision positioning, navigation and timing services, as well as Satellite-Based Augmentation System (SBAS) and Ground-Based Augmentation System (GBAS) services in the Asia area

around China [4–6]. The precision of the estimated satellite clock offset is essential to time synchronization [7], and an important prerequisite for the realization of real-time Precise Point Positioning (PPP) is the estimation of real-time satellite clock offset. The popular autonomous driving technology and BDS wide-area augmentation system cannot be fulfilled without the support of real-time clock offset corrections [8].

Precise clock estimation is the foundation of GNSS application in both engineering and science [9,10]. Clock parameters and orbit parameters are estimated together in the process of satellite orbit determination, which suffers from a large number of estimable parameters, and the data processing period is usually too long to be applied to high-precision real-time clock offset estimation. Therefore, satellite clock offset is usually estimated separately by fixing satellite orbits, earth rotation parameters, station coordinates, etc. in current studies. This method, thanks to the improvement in the calculation efficiency and reduction of the number of parameters, can estimate the precise satellite clock offset in real-time. Hauschild et al. proposed a GPS satellite clock offset estimation algorithm by processing the un-differenced range and carrier-phase observations of the global network, and the accuracy of calculated satellite clock offset was 0.20–0.43 ns [11]. Zhang et al. presented an efficient clock estimation approach efficiently and accurately generating a 1 Hz clock by combining un-differenced (UD) and epoch-differenced (ED), and the clock estimation accuracies were within 0.1 ns [12]. Huang et al. proposed a new method that can automatically detect outliers and clock jumps in real-time and thus has an eximious performance [13]. Chen et al. presented a modified mixed-differenced (MD) approach for estimating GPS, BDS, Galileo and GLONASS real-time clock offset, and except for the BDS GEO satellites, the Standard Deviations (STD) of the four-systems clock offset are approximately from 0.1 to 0.4 ns [14].

A huge number of related research has focused on BDS satellite clock offset, for instance, estimating real-time clock offset or analyzing the physical characteristics of the atomic clocks [15]. Fu et al. presented a sequential least squares method for estimating BDS real-time satellite clock offset, and the STD of the estimated clock is 0.17 ns [16]. Kuang et al. developed an uncombined model for the estimation of a BDS-3 multi-frequency real-time clock, and the STD of the double-differenced clock was generally less than 0.05 ns [17]. A series of research on the physical characteristics of atomic clocks show that the quality of BDS-3 atomic clocks is greatly improved compared with BDS-2, but the clock offset and frequency of BDS-3 still exist jumps, and the frequency drift varies in range from -2×10^{-18} to 2×10^{-18} s/s^2 [18]. About 70% of BDS-3 positioning solutions are within 0.7 m at 10 min thanks to the improvement in the BDS-3 atomic clock stability [19].

Most of the achievements on the BDS precision clock offset estimation focus on using the global network; however, the local area network is rarely involved. This is because the local area network is limited by the regional observation environments, and the overall arc observation of satellites is not as good as that of the global tracking network; therefore, the accuracy of the clock offset is affected. However, stations are not sufficient to observe BDS compared with other GNSS systems among the Multi-GNSS Experiment (MGEX) stations, hence studying the calculation of BDS satellite clock offset is significant in the use of the local area networks. The observation data in the Asia-Pacific is used to calculate the BDS regional real-time clock offset in this article. Then, this study compares the accuracy of clock offset estimated in the Asia-Pacific with that of the global region to analyze the accuracy and performance of the clock offset regional calculation. More importantly, starting from the characteristics of the atomic clocks, this article analyzes the performance of BDS clock offset calculation, which compensates for the defect that the existing research rarely deals with the other potential reasons for the fluctuation of BDS clock offset accuracy.

In this manuscript, we estimated the BDS real-time clock offset using the MD model based on the global and Asia-Pacific observation data, taking the advantages of the UD model and the ED model into account. The MD model not only introduces the initial deviation as a datum to improve the accuracy, but also improves the computational efficiency. Efficient estimation of real-time satellite clock offset is achieved without fixing clock deviation, and the estimated BDS clock offset is compared with the precise clock

product of Geo Forschungs Zentrum (GFZ) to evaluate the quality of the estimated BDS clock offset by using the quadratic difference method. Furthermore, the parameters of the BDS space-borne atomic clock are obtained by fitting the GFZ post-processing precise clock, and the calculation quality of the BDS real-time clock offset is explained by analyzing the characteristics of atomic clocks.

The remaining chapters of our research are as follows: In Section 2, the existing clock offset estimation models and their advantages and disadvantages are introduced, as well as the comparison between the models. The clock offset estimation results of global/Asia-Pacific BDS satellites are analyzed, and the accuracy achieved by each orbit type satellite is counted in Section 3. Subsequently, by fitting the precise clock product of the GFZ analysis center, the physical characteristic parameters of the satellite clock offset are obtained to explain the solution of the real-time estimated clock offset. Thereafter, the positioning accuracy of kinematic PPP is evaluated in Section 4. Finally, some conclusions are summarized.

2. Methodology

2.1. Un-Differenced Approach

The UD method estimates the precise clock offset using the ionosphere-free phase, pseudo-range observations, fixing satellite orbits and precise station coordinates [12]. The errors such as phase center deviation, earth solid tide, phase rotation and relativistic effects are corrected by the empirical models. The corresponding observation equations are as follows:

$$v_{Lc}(i) = \widetilde{t}_r(i) - \widetilde{t}_s(i) + M(i)d_{trop}(i) + N + l_{Lc}(i) \quad (1)$$

$$v_{Pc}(i) = \widetilde{t}_r(i) - \widetilde{t}_s(i) + M(i)d_{trop}(i) + l_{Pc}(i) \quad (2)$$

where v_{Lc} is the residuals of the ionosphere-free carrier phase, and v_{Pc} is the residuals of the pseudo-range observations, respectively; i is the epoch; and $\widetilde{t}_r$ and $\widetilde{t}_s$ are receiver and satellite atomic clock parameters, respectively; M and $d_{trop}(i)$ represent the mapping function and Zenith Total Delay (ZTD) parameter; N represents the ambiguity of the carrier phase observations; l_{Lc} and l_{Pc} are the difference between the observation and the geometric distance.

The UD model retains the ambiguity parameters, which can provide convenience for subsequent dual-difference ambiguity resolution and satellite hardware delay deviation estimation. However, it must estimate several parameters due to the existence of ambiguity, which is computationally inefficient.

2.2. Epoch-Differenced Method

The ED model eliminates the ambiguity parameters by making differences between two adjacent epochs, which greatly improves the calculation efficiency because of the reduced number of estimable parameters [20]. The observation equations for estimating epoch-differenced phase and undifferenced range are as follows:

$$v_{\delta Lc}(i) = \delta\widetilde{t}_r(i) - \delta\widetilde{t}_s(i) + \delta M(i)d_{trop}(i) + \delta l_{Lc}(i) \quad (3)$$

$$v_{\delta Pc}(i) = \delta\widetilde{t}_r(i) - \delta\widetilde{t}_s(i) + \delta M(i)d_{trop}(i) + \delta l_{Pc}(i) \quad (4)$$

where δ represents the difference operator. The ED model eliminates the ambiguity parameter in the observation, leaving differenced clock and differenced ZTD of the two adjacent epochs. The clock offset between epochs must be accumulated to obtain clock correction. About $\delta\widetilde{t}(i)$, there is

$$\widetilde{t}(i) = \widetilde{t}(i_0) + \sum_{j=i_0+1}^{i} \delta\widetilde{t}(j) \quad (5)$$

The accumulated clock correction can be estimated accurately despite the clock offset change, which is the deviation of the clock offset $\delta\widetilde{t}(i_0)$ at the start epoch i_0.

However, the data utilization of this method is inefficient, and the ED model generates relative clock offset. Therefore, obtaining the required satellite clock offset needs to introduce an initial datum, which is unlikely to be accurately obtained, and thus there will be a certain deviation. Meanwhile, making a difference between epochs will increase the correlation of the observations.

2.3. Mixed Differenced Model

According to Sections 2.1 and 2.2, the ED method has fewer parameters to be estimated and is efficient and timely, which can achieve the real-time 1 Hz clock. However, the introduced initial satellite clock offset inevitably contains deviation. The initial bias for each clock can be sufficiently determined by the UD pseudo-range observation [20]. In this paper, the method combining the ED carrier phase difference and the UD range observations can accurately estimate the clock variation and clock deviation.

According to Equations (1)–(4), the observation equations of epoch-differenced phase and un-difference range can be obtained as follows:

$$v_{\delta Lc}(i) = \delta\widetilde{t}_r(i) - \delta\widetilde{t}_s(i) + \delta M(i) d_{trop}(i) + \delta l_{Lc}(i) \tag{6}$$

$$v_{Pc}(i) = \widetilde{t}_r(i) - \widetilde{t}_s(i) + M(i) d_{trop}(i) + l_{Pc}(i) \tag{7}$$

Starting from epochs i_{r0} and i_{s0}, the clock correction values $\widetilde{t}_r(i)$ and $\widetilde{t}_s(i)$ in Equation (7) are replaced by Equation (5).

$$v_{Pc}(i) = \delta\widetilde{t}_r(i) - \delta\widetilde{t}_s(i) + M(i) d_{trop}(i) + \widetilde{t}_r(i_{r0}) - \widetilde{t}_s(i_{s0}) + l_{Pc}(i) + \sum_{j=i_{r0}+1}^{i-1} \delta\widetilde{t}_r(j) - \sum_{j=i_{r0}+1}^{i-1} \delta\widetilde{t}_s(j) \tag{8}$$

The last three terms of Equation (8) are expressed as $\bar{l}_{pc}(i)$, and clock offset is replaced by epoch-difference value, it becomes

$$v_{Pc}(i) = \delta\widetilde{t}_r(i) - \delta\widetilde{t}_s(i) + M(i) d_{trop}(i) + \widetilde{t}_r(i) - \widetilde{t}_s(i_{s0}) + \bar{l}_{Pc}(i) \tag{9}$$

The ED method can precisely estimate the clock variation and ZTDs by using Equation (6). At the meantime, the range observations need to be corrected during data processing, in order that the subsequent solution only retain the initial clock biases. Substitute the clock change at epoch i into the accumulated clock difference, and obtain from Equation (8) as follows,

$$v_{Pc}(i) = \widetilde{t}_r(i_{r0}) - \widetilde{t}_s(i_{s0}) + l_{Pc}(i) + \sum_{j=i_{r0}+1}^{i} \Delta\widetilde{t}_r(j) - \sum_{j=i_{s0}+1}^{i} \delta\widetilde{t}_s(j) + M(i) d_{trop}(i) \tag{10}$$

After replacing last four terms by $\widetilde{l}_{Pc}(i)$, Equation (10) becomes

$$v_{Pc}(i) = \widetilde{t}_r(i_{r0}) - \widetilde{t}_s(i_{s0}) + \widetilde{l}_{Pc}(i) \tag{11}$$

To sum up, two steps of the data processing are estimating the ZTD parameters and clock variation using the ED of Equation (6), and estimating the initial clock bias using the UD of Equation (11).

The MD method takes both advantages of ED and UD into account, which not only improves the calculation efficiency, but is convenient for users to implement. However, the stability of the model might be affected by factors, for instance when satellites rise or set. Continuous satellite observations are required in the initialization of the clock offset. Only when the initial clock offset converges to the accuracy of the range observations can it be used to calculate clock offset. Once the observation is interrupted, the clock offset requires re-initialization, and with regard to the frequency of the re-initialization is related to the observations of each satellite for the station on one day. In addition, both the distribution of stations and the quality of the observation data as well as the geometry of satellites

have a certain influence on the estimate of the clock offset. Under the circumstance of reasonable spacing of observation stations, the estimated clock offset will achieve satisfying accuracy if there are massive observation stations with uniform distribution and good satellite geometry.

2.4. Efficiency of Different Models

Due to the huge estimable parameters, the real-time clock cannot reach the 1 Hz update rate using the UD model. The ED model can eliminate a mass of ambiguity parameters, and the calculation is efficient. However, the introduced initial satellite clock offset exists deviations. The MD model combines the characteristics of the two models. Therefore, as long as appropriate hardware and global stations are selected, the MD model can fully attain the increasing parameters of BDS-3 satellites or other GNSS systems to estimate real-time clock offset. Figure 1 shows the comparison between the number of stations and the number of estimated parameters.

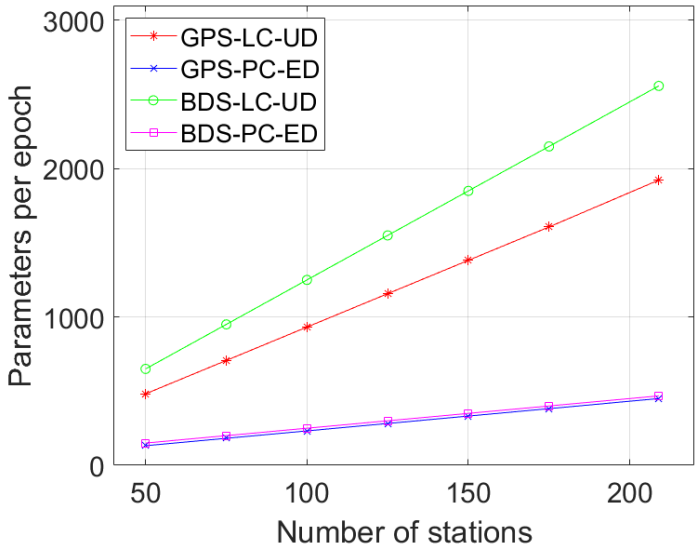

Figure 1. Efficiency of different models.

Figure 1 shows that the number of parameters of the UD model increases significantly with the increase of the number of stations and therefore the corresponding efficiency decreases. The number of parameters of the ED model increases not obviously, and it is relatively steady and efficient with a small increment. Currently, many countries are developing their own navigation systems and establishing corresponding stations, and therefore the number of stations is increasing. The MD model will improve the efficiency of multi-system and large-scale stations, and thus is a very suitable choice for estimating the real-time clock.

3. BDS-3 Satellite Clock Offset

In this chapter, the clock offset involved in Sections 3.1–3.3 are all real-time clock offsets, while only Section 3.3 uses the precise clock product because it can reflect the physical characteristics of the satellite atomic clocks. Section 3.3 aims to further explain the estimation quality of real-time clock offset in Sections 3.1 and 3.2

3.1. Data and Strategy

In order to analyze the feasibility of the estimation model for real-time precise clock offset in the global region and the Asia-Pacific, this experiment estimates two sets of clock products for comparison. The time range is from Day of Year (DOY) 214 to 243 in 2021. A total of 209 and 81 BDS stations are selected in the global and Asia-Pacific regions, respectively, and the distributions are shown in Figure 2.

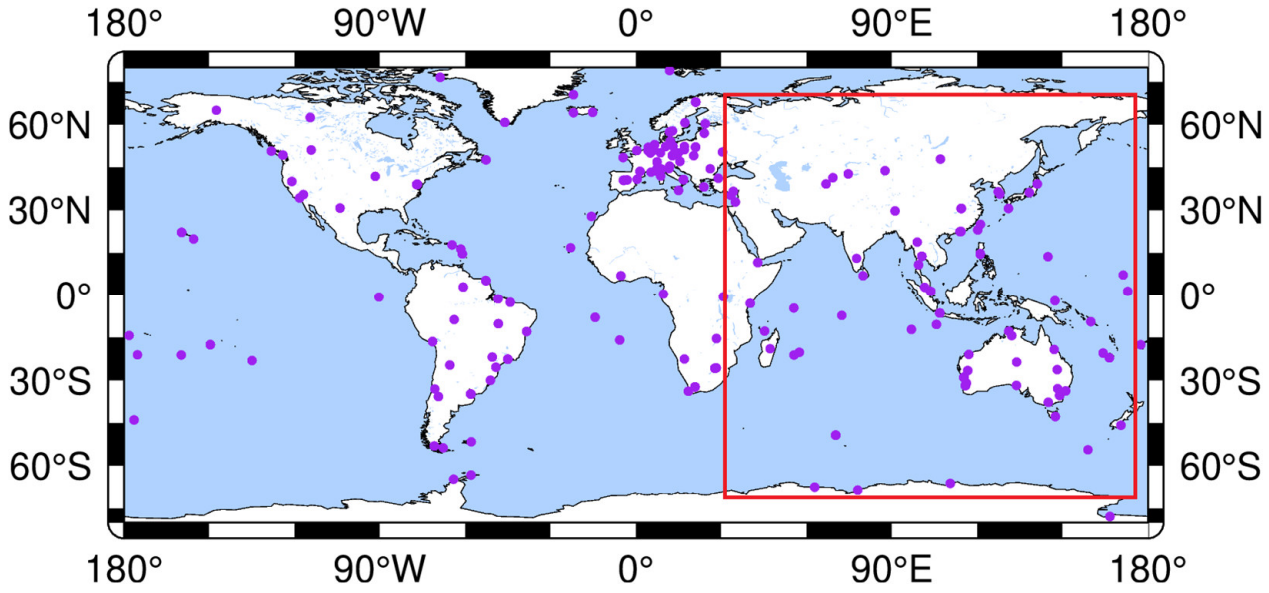

Figure 2. Distribution of the observable BDS stations in global (and the stations in Asia-Pacific are within the red rectangle).

Table 1 shows the data processing strategies of this experiment as follows:

Table 1. Estimation strategy of real-time clock offset.

Parameter	Strategy
Observations	UD range and ED phase
Cut-off elevation	7°
Observation weights	Elevation-dependent weight
Intervals	1 s
Earth solid tides	IERS conventions 2010 [21]
Ocean tides	IERS conventions 2010 [21]
Phase wind-up	Corrected [22]
Satellite PCV	uncorrected
GEO satellite PCO	IGS14.atx [23]
IGSO/MEO satellite PCO	ESA Mode [24]
Receiver PCV/PCO	IGS14.atx
Relativistic effects	Correct
Reference clock	Receiver with stable atomic clock (e.g., PARK)
Adjustment model	Square root information filtering [25]
Ephemeris	Ultra-rapid ephemeris of GFZ
Tropospheric delay	Saastamoinen model [26] + GMF mapping function random-walk process [27]
Satellite/Receiver clock	Estimated as white noise
Station coordinates	Fixed

To analyze the impact of satellite generations and atomic clock types, the information of the current BDS satellites in orbit is listed in Table 2, including system generations (BDS-2, BDS-3), orbit type (GEO, IGSO, MEO), satellite pseudo random noise code (PRN), and atomic clock type (Rb, PHM). This experiment involves BDS-3 with a total of 17 PHM atomic clocks and 12 Rb atomic clocks, and all 15 BDS-2 atomic clocks are Rb atomic clocks. Table 2 shows the satellites' detailed information.

Table 2. Detail information of BDS satellites [28].

Satellite Generations	Orbit Type	PRN	Clock Type
BDS-2	GEO IGSO MEO	C01 C02 C03 C04 C05 C06 C07 C08 C09 C10 C13 C16 C11 C12 C14	Rb
BDS-3	GEO IGSO	C59 C60 C38 C39 C40	PHM
	MEO	C19 C20 C21 C22 C23 C24 C32 C33 C36 C37 C45 C46	Rb
		C25 C26 C27 C28 C29 C30 C34 C35 C41 C42 C43 C44	PHM

3.2. Estimated BDS-3 Clocks

The fixed GFZ orbit is used to obtain the real-time satellite clock offset, and the quadratic difference method [29] is applied to analyze the real-time BDS clock offset with the GFZ precise clock product. The STD is calculated every day to evaluate the accuracy of the estimated real-time clock offset [30]. This experiment selects C25 as the reference satellite for the clock offset estimated in the global to make a difference because of its stable performance, while the reference satellite for the clock offset estimated in the Asia-Pacific comparison is selected according to the principle of the longest visible arc. Figure 3 shows the daily scatter plot of the estimated clock offset accuracy, which can roughly reflect the calculation situation of each satellite every day.

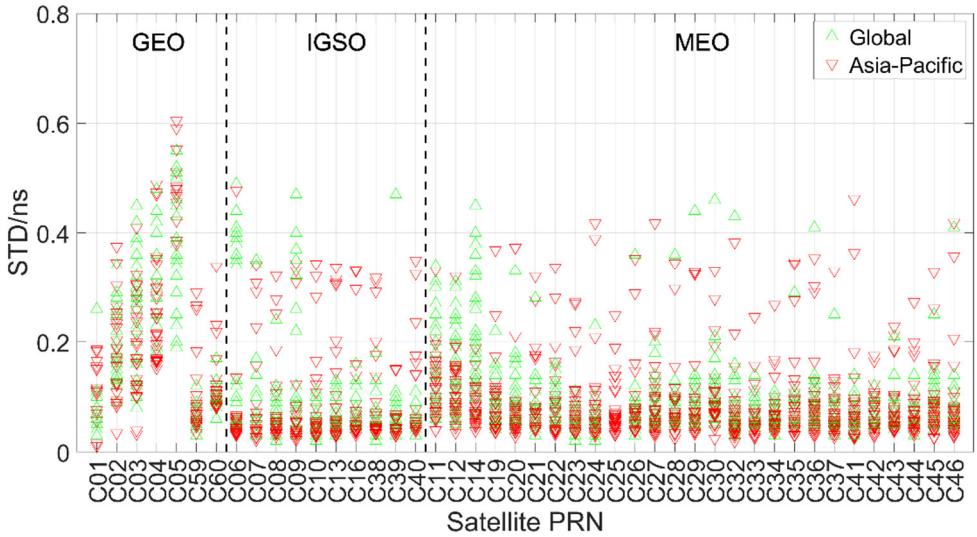

Figure 3. Daily accuracy of BDS clock offset in Global (green triangle) and Asia-Pacific (red triangle).

From Figure 3, we can see that most clock offset results estimated in the global are more concentrated than that of the Asia-Pacific. The reason that the clock offset results estimated in the Asia-Pacific are slightly dispersive is due to the fewer regional stations, the shorter arcs involved in the calculation, and the poor continuity of the observation data. For more comparison and convenient statistics, the calculation results of each BDS satellite in DOY 214–243 are averaged to obtain the accuracy of multiple days, as shown in Figure 4. The satellite number marked as bright cyan indicates the BDS-2 satellites, while the satellite number of BDS-3 satellites are presented in black.

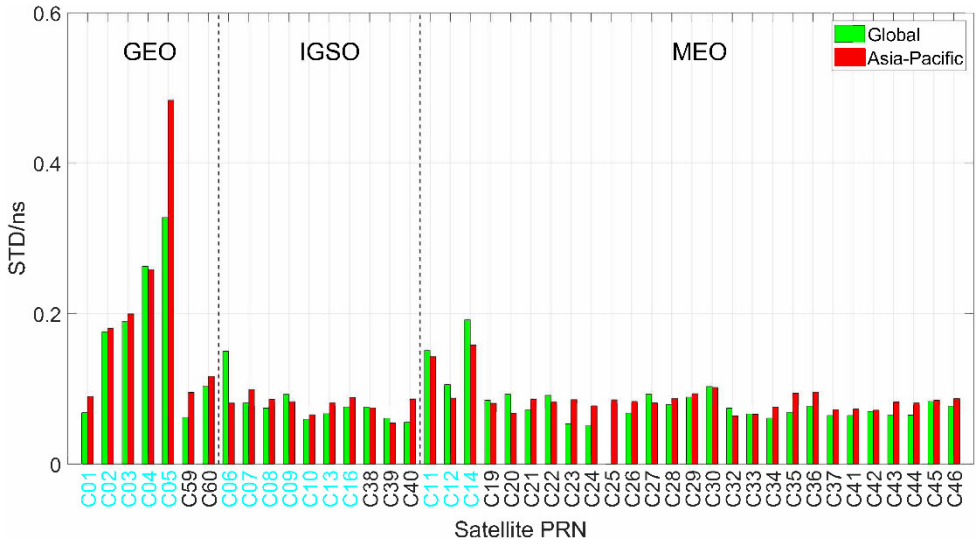

Figure 4. Global/Asia-Pacific mean precision of BDS clock offset in DOY 214–243.

From Figure 4, we can see that the accuracy of the BDS IGSO and MEO satellite clock offset estimated in global are within 0.2 ns. The same goes for the clock offset estimated in Asia-Pacific. The clock offset estimated in both areas have single-day results over 0.2 ns in Figure 3, which is related to the quality of observations. The overall clock offset accuracy of BDS-2 GEO satellites are worse than that of BDS-3. The GEO satellites of the BDS system are synchronous fixed-point, and the layout and design are to support the short message service of BDS-3. Therefore, the value of the clock offset estimation and other research aspects are less important.

The C05 clock offset result is worse than other GEO satellites because the clock offset had no results from 11:30 a.m. to 12:30 p.m. in DOY 237, and an obvious leap occurred at 12:30 p.m. The leap has a great impact on the processing of the subsequent data. There was no orbit data for about half an hour on that day in the IGS multi-system broadcast ephemeris either, and there was a significant leap before and after the interruption. In addition, this problem caused the GFZ precise clock file of DOY 237 to be ineffective, while this problem did not exist on other dates. From this point of view, the broadcast ephemeris not only has an impact on this experiment, but also on the products of the GFZ Analysis Center.

The estimation accuracy of satellite clock offset for each orbit type in Global and Asia-Pacific is shown in Table 3.

Table 3. BDS-2/3 clock offset accuracy statistics of various orbits in Global/Asia-Pacific (unit: ns).

Orbit Type	Global (BDS-2/BDS-3)	Asia-Pacific (BDS-2/BDS-3)
GEO	0.171 (0.207/0.083)	0.204 (0.243/0.106)
IGSO	0.072 (0.076/0.064)	0.077 (0.079/0.072)
MEO	0.082 (0.126/0.075)	0.085 (0.103/0.082)
Mean	0.093 (0.130/0.074)	0.102 (0.138/0.082)

According to the statistics results of the experiment in Table 3, the BDS clock offset are stabilized and satisfy the accuracy requirements except for BDS-2 GEO satellites. The average accuracies of estimated satellite clock offset of three orbit types with GEO, IGSO, and MEO in the Asia-Pacific area are 0.204 ns, 0.077 ns, and 0.085 ns, respectively, which can achieve a comparable accuracy of 0.171 ns, 0.072 ns and 0.082 ns with the globally estimated satellite clock offset. The GEO clock offset has the worst calculation results among those three orbit types. IGSO and MEO satellites' clock offset are pretty good compared with GEO. This is because IGSO and MEO satellites have superior geometry than GEO satellites. Because of the distribution of GNSS stations and the duration of valid observation data,

the accuracy of the clock offset estimated in the Asia-Pacific is slightly worse than that of the global.

As can be seen from Figure 1, the number of calculation parameters rise with the increasing stations. Combining the above calculating result of the clock offset, the calculation parameters in the Asia-Pacific are less than that of global estimation. The Asia-Pacific clock estimation is equivalent to the global with less calculated time. It can not only reduce the time required for the solution calculation, but also satisfy the demand of the precise clock offset. The average accuracy of the BDS-3 satellite clock offset is generally better than that of the BDS-2. The reason is that the BDS-2 satellites were launched earlier, and the aging hardware would lead to the instability characteristics of the satellite atomic clock. However, PHM clocks installed on BDS-3 satellites have better performance. The following section will analyze the atomic clock parameters in detail.

3.3. Characteristics of BDS-3 Atomic Clock

The new generation BDS-3 satellites include two types of atomic clocks, namely new Rb and PHM clocks. In order to analyze the reasons for the unsatisfactory calculation of several satellite clocks offset, we use the quadratic polynomial model to fit various parameters of BDS precise satellite clock offset to reflect the physical characteristics of atomic clocks, and the equation of polynomial model is as follows [31]

$$C_i = b_0 + b_1(t_i - t_0) + b_2(t_i - t_0)^2 + \varepsilon_i,\ i = 1, 2, 3 \ldots, n \tag{12}$$

where the coefficients $b_0,\ b_1,\ b_2$ are obtained by fitting the precision clock using the polynomial, and b_0 represent the phase, b_1 represent the frequency, and b_2 represent the frequency drift. ε_i is the fitting residual; n is the number of clock epochs; C_i is the clock data.

The globally estimated satellite clock offset has sufficient data as compared to that of the Asia-Pacific, and thus this paper selects the former dataset to study and analyze the physical characteristics of satellite atomic clocks. In the following, GEO satellites are presented in red, IGSO satellites in blue, and MEO satellites in green. The Rb atomic clocks are marked in orange, and the PHM atomic clocks are marked in manganese violet.

3.3.1. Phase Series

The phase series of each BDS satellite atomic clock are obtained by fitting the precision clock as shown in Figures 5 and 6. It can be seen that the phase series of BDS satellite atomic clocks jumps in some periods.

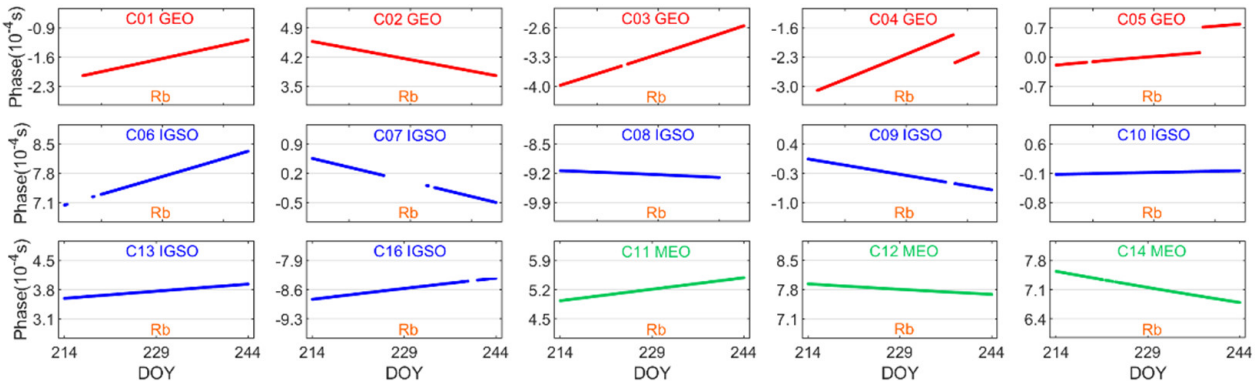

Figure 5. Phase series of BDS-2 satellites.

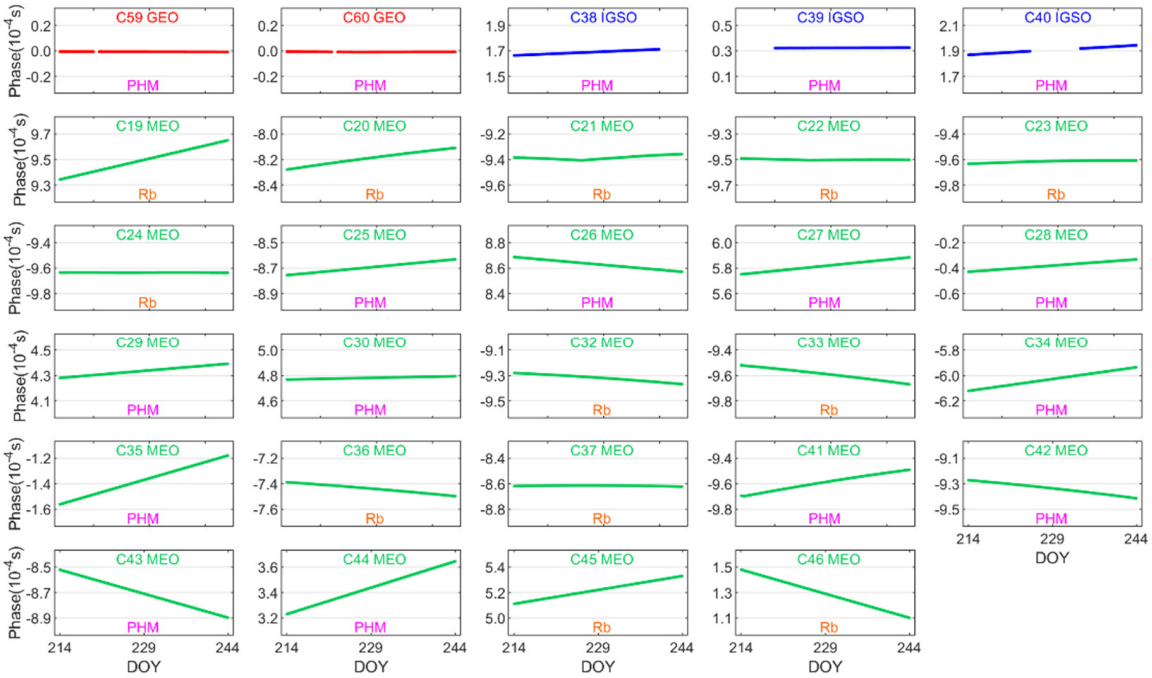

Figure 6. Phase series of BDS-3 satellites.

Both BDS-2 C04 and C05 jump, while the BDS-3 satellites and other BDS-2 satellites are stable. It can be seen that C21, C22, C23, C24, C37 Rb atomic clocks own the nonlinear phases series, while the phases of PHM atomic clocks are all linear trends. That means the PHM clocks show good long-term continuity. The primary cause of phase jumps is that the ground control station actively adjusts the phase to guarantee the time synchronization error between the satellite and the station within a predetermined threshold. However, the continuity of satellite atomic clocks will be disrupted by these phase adjustments.

3.3.2. Frequency Series

Figures 7 and 8 show the frequency series of the BDS satellite atomic clocks. It can be seen that the frequency jumps or the slope changes in some periods, which affect the service performance and continuity of atomic clocks. The slope of the frequency series will not change after active frequency adjustment. If the slope of the frequency series changes, it can be inferred that the onboard atomic clock has switched between the master and the backup clock.

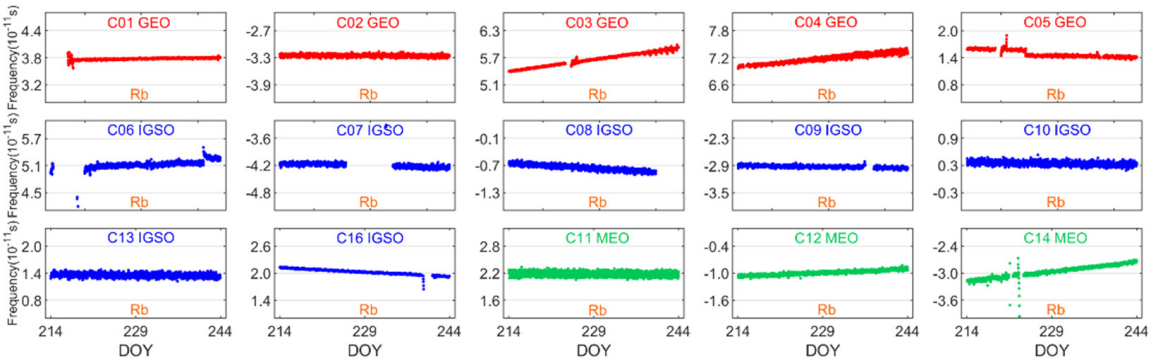

Figure 7. Frequency series of BDS-2 satellites.

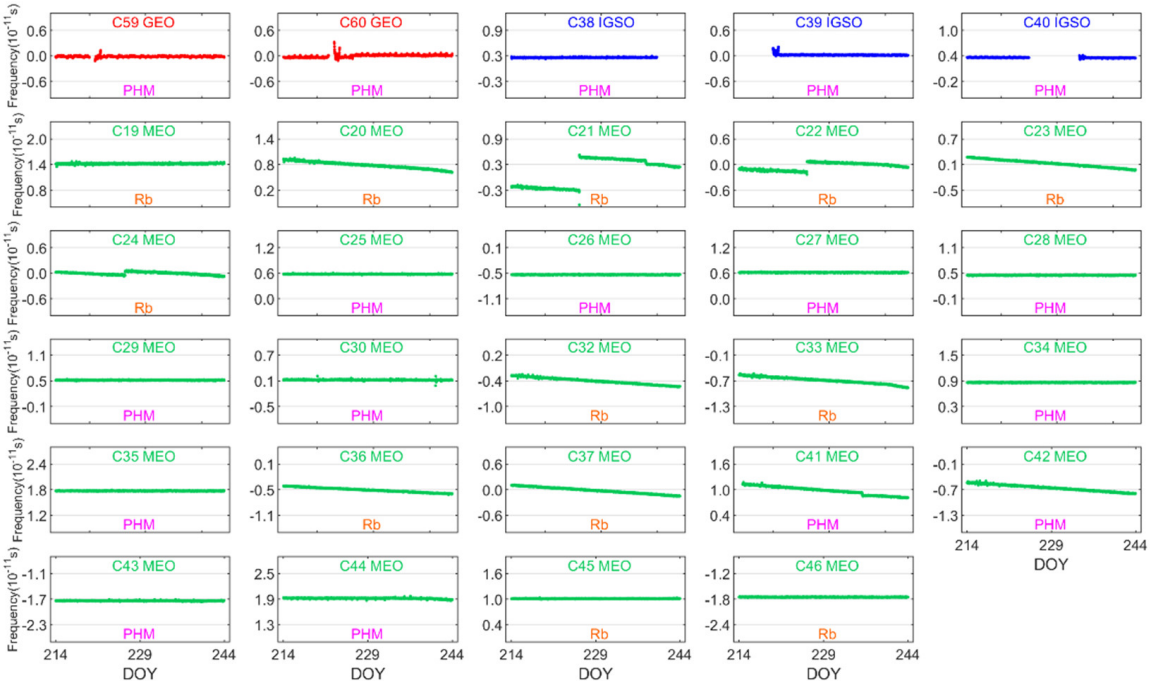

Figure 8. Frequency series of BDS-3 satellites.

Most of the frequency changes of BDS-2 clocks are in the range of 0~1 $\times$ 10^{-11}. The frequency series of C05 and C06 have a lot of discrete points, and this may be one of the reasons for not being well estimated. C14 has large fluctuations in some periods, which may be because the accuracy of their clock products is low, and only a few stations can track C14. Therefore, C14 is not as stable as other satellites.

From Figure 8, it can be seen that the variation range of the BDS-3 clocks frequency series is basically within the range of 0~0.6 $\times$ 10^{-11}, which is smaller than that of BDS-2. BDS-3 clocks are stable with concentrated frequency series. When the frequency of C21 changes, the slope of the corresponding phase also changes in Figure 6. The purpose of frequency adjustment is to control the time deviation between the satellite atomic clock and the BDS system within a range so as to avoid the gradual increase of the time deviation caused by the frequency drift of the satellite atomic clocks, which would affect the user's service performance.

3.3.3. Frequency Drift Series

The frequency drift series for BDS clocks are shown in Figures 9 and 10, and they maintain on the order of 1 $\times$ 10^{-18}, varying from -7 to 7 $\times$ 10^{-18}. The frequency drift represents the aging rate of the atomic clocks.

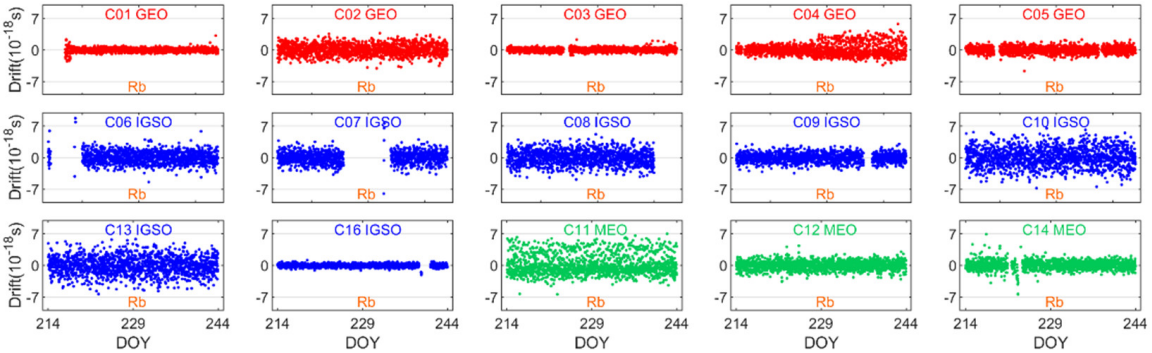

Figure 9. Frequency drift series of BDS-2 satellites.

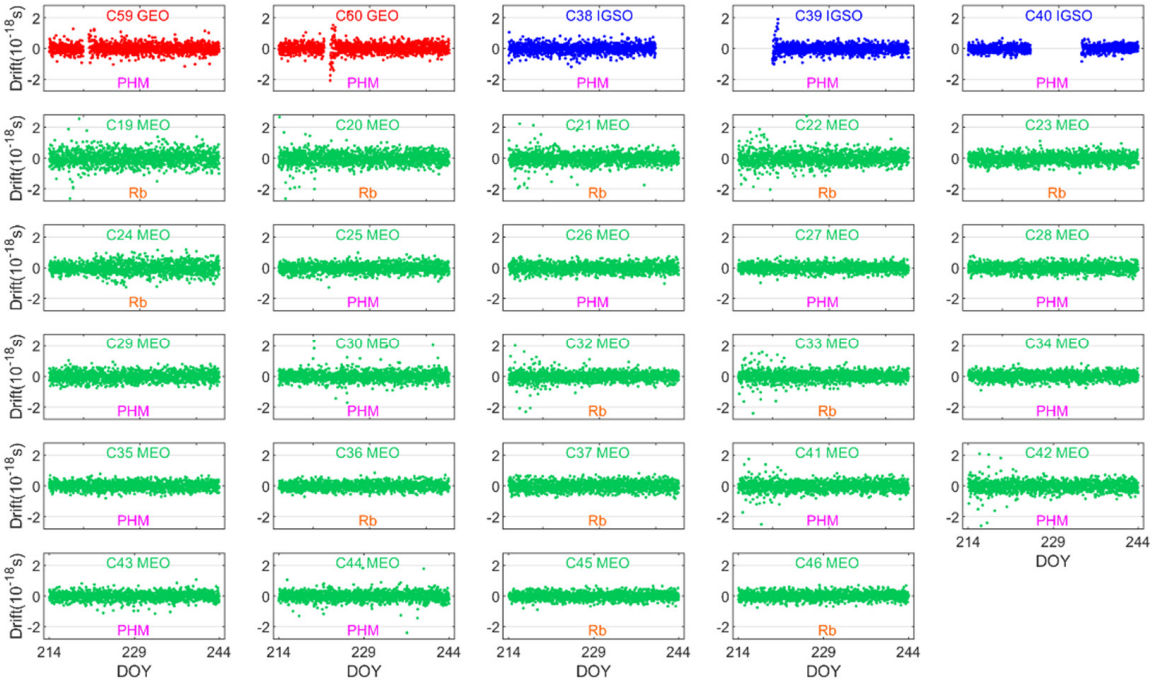

Figure 10. Frequency drift series of BDS-3 satellites.

The frequency drift series of BDS-3 are more stable than that of BDS-2 and are basically in the range of -2~2×10^{-18}. Frequency drift series of C10, C11, C13 are more concentrated than other same-type satellites. The dispersion of the frequency drift series of BDS-3 satellite atomic clocks are smaller than that of BDS-2, and the distribution of BDS-3 is obviously more concentrated and converging to zero than that of BDS-2. Due to the aged satellite hardware, the frequency drift series of BDS-2 satellites have some fluctuations, while BDS-3 clocks do not fluctuate significantly. This can indicate that the BDS-3 atomic clocks have a slower aging rate and the hardware of BDS-3 is more suitable for long-term service. Meanwhile, PHM atomic clocks are more stable than Rb atomic clocks.

3.3.4. Residual and Fitting Precision

The fitting precision is evaluated by calculating the RMS of the residual. Figures 11 and 12 show the residual series of the BDS clocks by fitting the second-order polynomial.

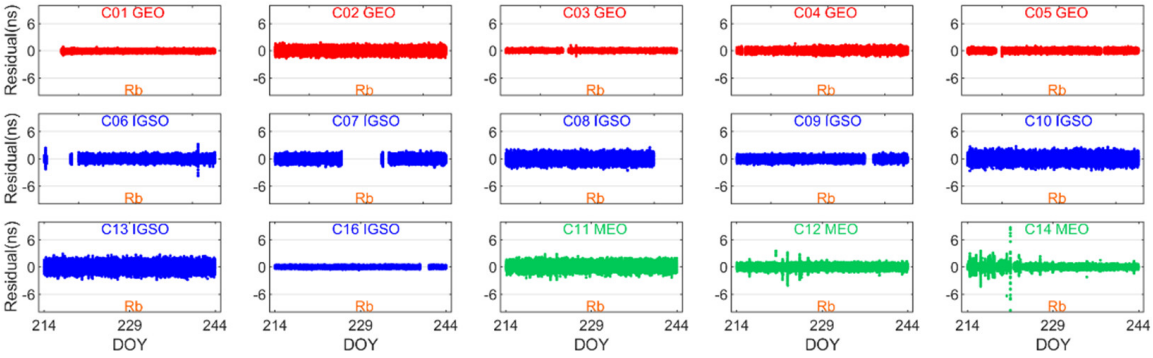

Figure 11. Fitting residual series of the BDS-2 satellites.

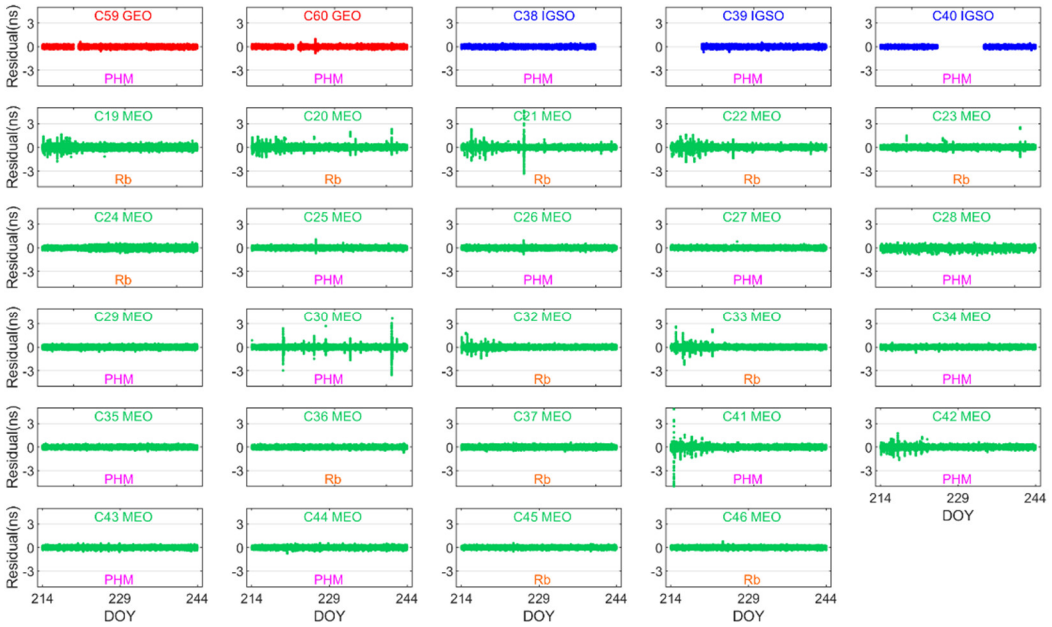

Figure 12. Fitting residual series of the BDS-3 satellites.

As we can see from Figures 11 and 12, the BDS atomic clocks have a good fitting result, which is within −3~3 ns. However, the residual series of C14, C21, C30, C41 are inconsistent. The unsatisfactory fitting residual may be due to the quality of the clock product or the physical characteristics of the clocks. In order to compare and analyze the performance of different clock types, including BDS-2, BDS-3, Rb and PHM, the RMS of fitting residuals is calculated separately, as shown in Figure 13.

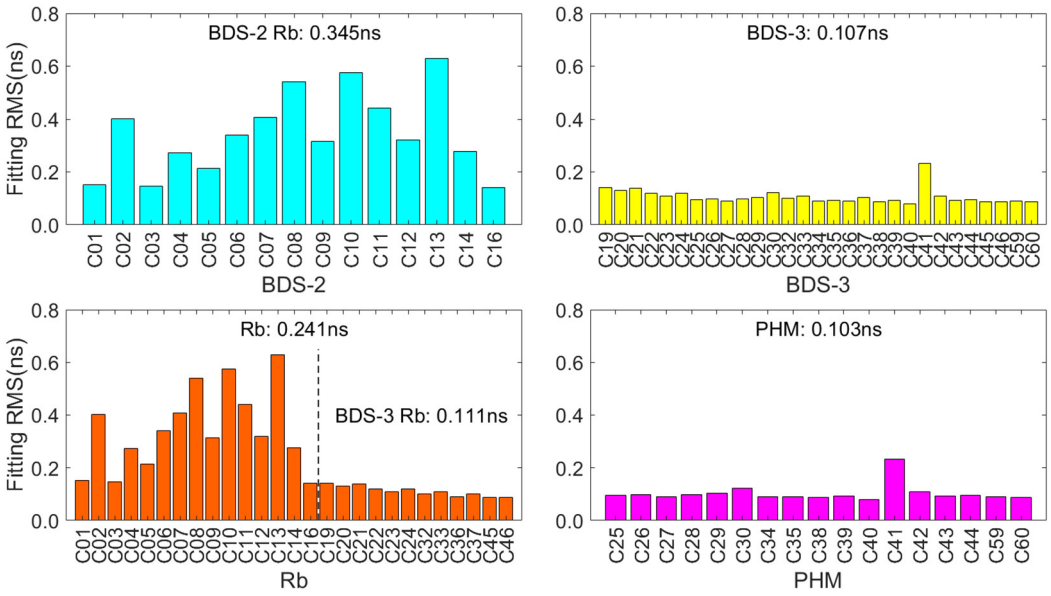

Figure 13. RMS of BDS clocks fitting residuals of different types.

The results are consistent with Sections 3.3.1–3.3.3. The fitting performances of BDS-3 atomic clocks are better than that of BDS-2 atomic clocks, which reflects that the satellite atomic clock carried by BDS-3 has better performance and is more stable than that of BDS-2. Simultaneously, the fitting result of the PHM clocks is much better than that of the Rb clocks, which indicates that the PHM atomic clocks are stable and can be fitted more accurately.

4. Kinematic PPP Validation

4.1. Positioning Data

Based on the clock estimations above, kinematic PPP was performed to test the positioning performance of the estimated clock offset in different areas by using the ultra-rapid ephemeris of GFZ. The ambiguity adopted float values, and other details of the kinematic PPP strategy is the same to the clock offset estimation strategy (see Table 2). The observations from DOY 225–231 were processed. Positioning errors of each epoch are calculated by fixing coordinates as references. 12 IGS multi-GNSS stations are selected for the positioning experiments. The distribution of these stations is listed in Figure 14.

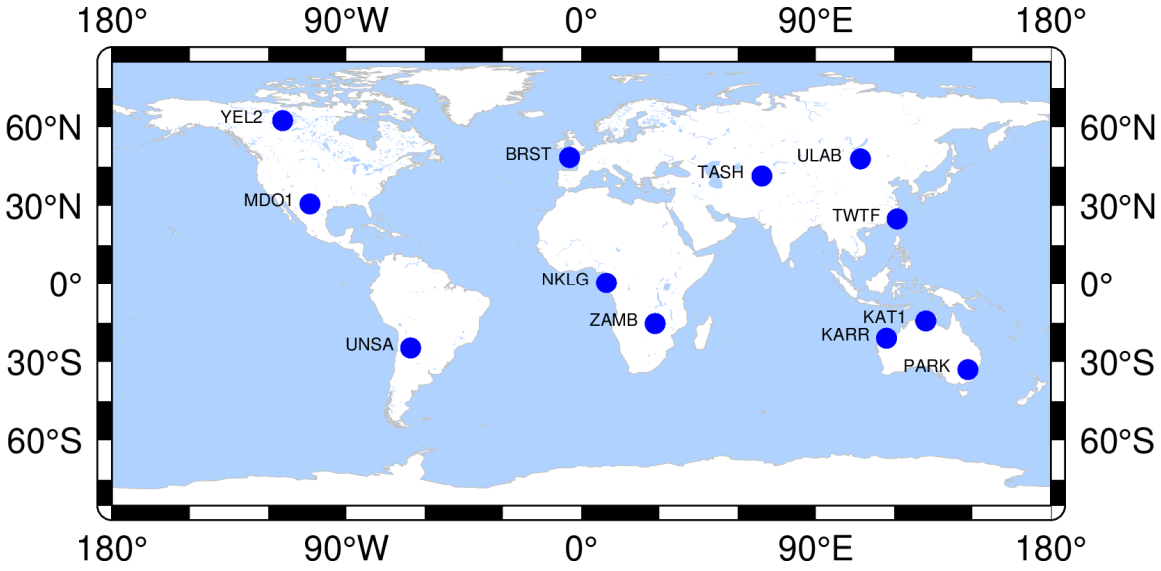

Figure 14. Distribution of stations for kinematic PPP validations.

The number of available BDS satellites varies in different areas, and its global distribution is shown in Figure 15.

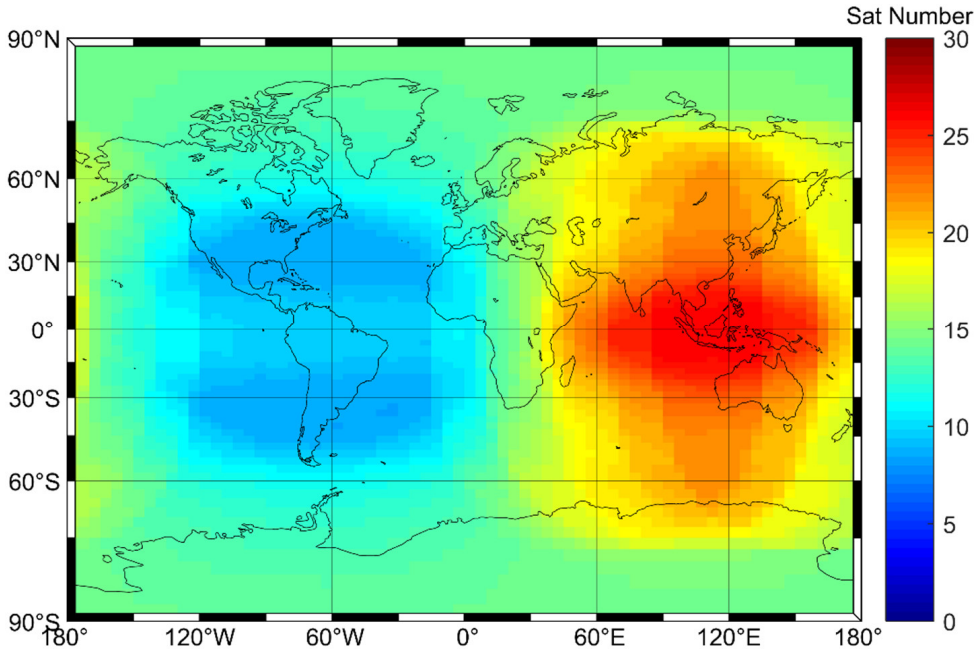

Figure 15. Global distribution of BDS satellite visibility.

From Figure 15, we can see that the number of available BDS satellites in the Asia-Pacific is larger than that in other areas. In Asia and Australia, the visible number of BDS satellites is greater than 18, which is significantly higher than that in other areas. Only parts of Africa, Europe and Antarctica can observe more than 15 BDS satellites, and most of the Americas has less than 15 satellites, and thus the visibility of BDS satellites is not as good as in the Asia-Pacific region. The reason is that GEO and IGSO satellites mainly cover the Asia-Pacific region.

4.2. Kinematic Positioning Results

The convergence is defined as the positioning deviation of horizontal directions and the vertical direction within 10 cm for 20 consecutive epochs, and the RMS of positioning deviation after the convergence of kinematic positioning is regarded as the positioning accuracy. The clock offset estimated in the global and Asia-Pacific is used to participate in the kinematic PPP, and some representative positioning results are shown in Figures 16 and 17.

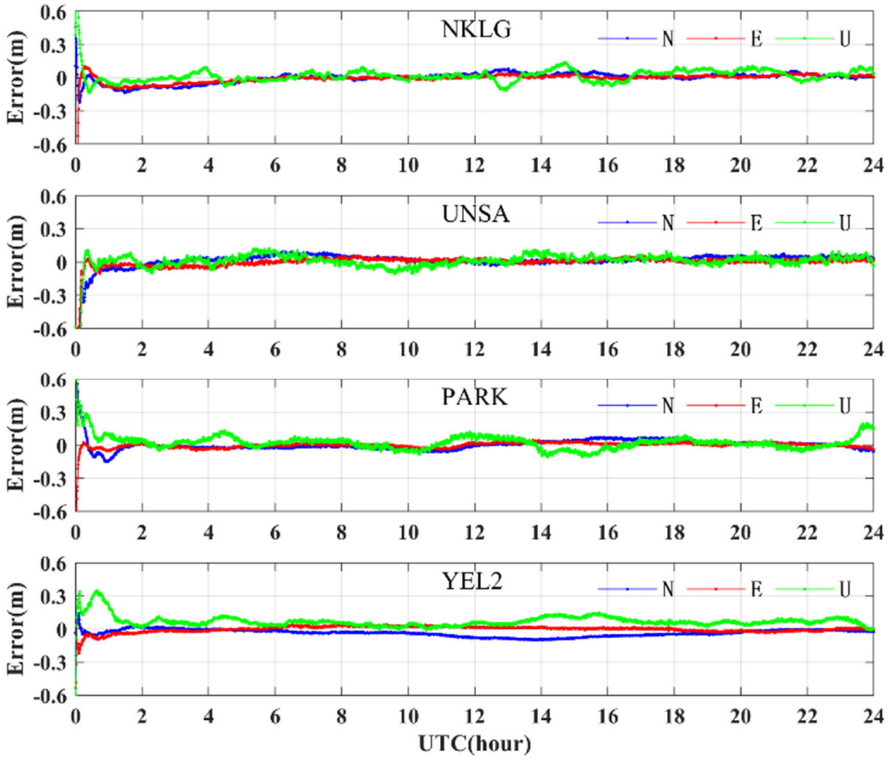

Figure 16. Kinematic PPP results using clock offset estimated in global.

It can be seen from Figures 16 and 17 that the BDS positioning results fluctuate in the U direction and are not smooth as in the N and E directions, and the overall positioning results using the regional clock offset are not as steady as using the global clock offset. Among regional positioning experiments, several station positioning results jump in some epochs because the BDS clock offset estimated in Asia-Pacific is incomplete continuity, and the clock offset involved in positioning is less than the clock offset estimated in global.

It is worth noting that the accuracy is obtained by averaging one week PPP results, and Figure 18 shows the specific positioning accuracy. For the convenience of comparison, the six stations in the picture below correspond to the six stations on the left side of the above picture, all of which are in the Asia-Pacific.

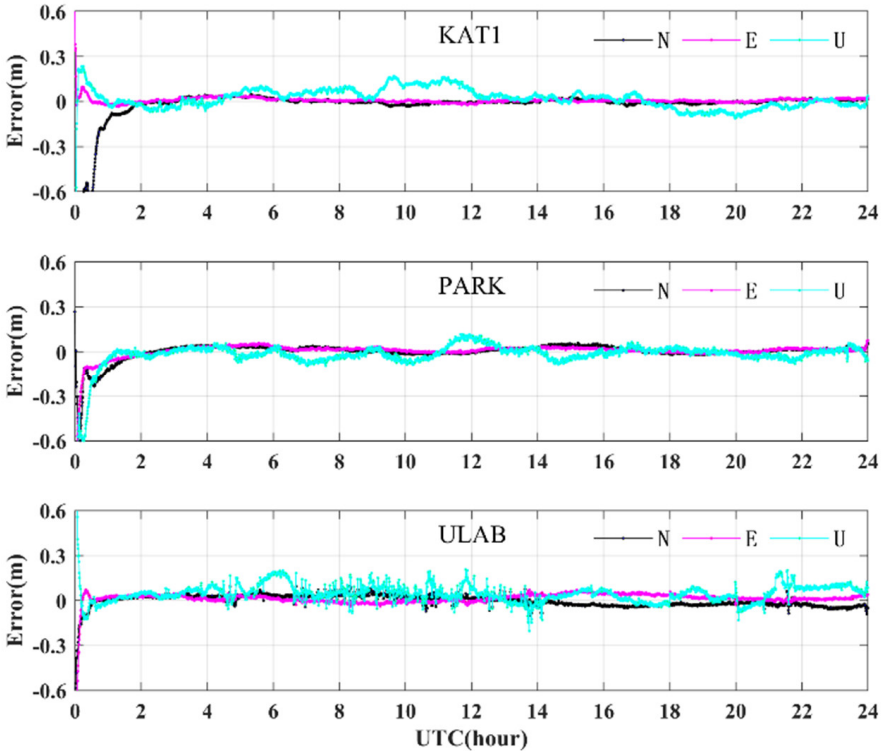

Figure 17. Kinematic PPP results using clock offset estimated in Asia-Pacific.

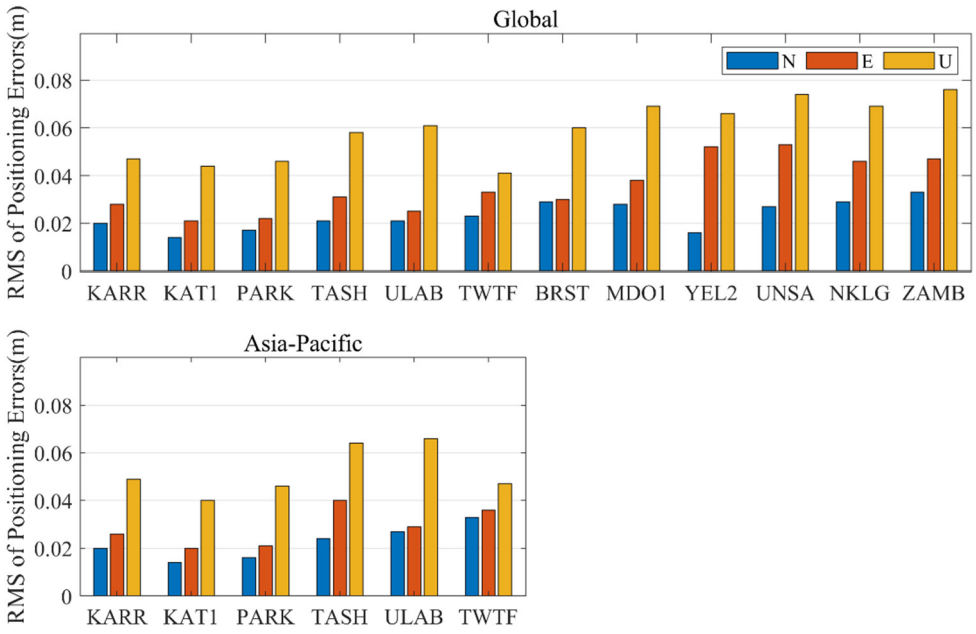

Figure 18. Kinematic PPP results using a different clock offset.

Figure 18 shows that BDS kinematic PPP results of global stations can achieve an average accuracy of 2.3, 3.6 and 5.9 cm in the N, E and U directions, which is satisfying for global kinematic positioning users. The kinematic PPP accuracy of stations in the Asia-Pacific, which involved the estimated clock offset in global and Asia-Pacific, is 1.9, 2.7, 4.9 cm and 2.2, 2.9, 5.2 cm in the N, E and U directions, respectively. The reason that the kinematic PPP results calculated by the Asia-Pacific estimated clock offset perform better than the clock offset estimated in global is that the BDS positioning accuracy in the Asia-Pacific is better than global mean accuracy, which is calculated by averaging the results of all stations. The

globally estimated clock offset is still slightly better if we only consider the PPP results of the stations in Asia-Pacific. The kinematic PPP convergence time of stations in global and Asia-Pacific is 36.49 min and 43.13 min, respectively. The main reason for the long convergence time of positioning in the Asia-Pacific is the small volume of clock offset data estimated in the Asia-Pacific. However, the performance of BDS Asia-Pacific estimated clock offset in kinematic PPP in Asia-Pacific is comparable to that of the globally estimated clock offset, which can provide reliable and high-quality services for users.

5. Discussion

According to the results, both the clock offset estimated in Asia-Pacific and global have good agreement with the precise clock product provided by the GFZ analysis center. Less stations but more BDS satellites are used in the estimation of clock offset in Asia-Pacific compared with the estimation of clock offset in global, and the accuracy that can be achieved of the former is slightly worse than that of the latter. The two sets of clock products have the same regularity that the accuracy of both MEO and IGSO satellites clock offset are equivalent and better than that of GEO satellites; in the meantime, overall BDS-3 satellites perform better than BDS-2 satellites. This work fills the gap of the clock offset estimated in the local area network. From a new perspective, the physical characteristic parameters, which represent the stability of atomic clocks, are obtained by fitting the corresponding precise clock offset to analyze the estimation results of the clock offset. The results show that the characteristics of the PHM atomic clocks are more stable than those of the Rb, and in the Rb atomic clocks, the BDS-2 satellites are not as good as those of the BDS-3. The positioning results by applying different clock offset products present that the Asia-Pacific is able to achieve a comparable positioning accuracy to the global. Both the accuracy of clock offset and positioning are almost equally matched with those of previous studies.

However, the regional estimation of satellite clock offset is discontinuous, as it has to cope with the satellites' rise and set and faces a smaller number of observations than that of global, which has the same impact on positioning, because it does not contribute as much compared with the global solution. In addition, there may be a certain lag in the analysis of the real-time clock offset solution by using the precise clock offset, since the situation can only be understood after the precise clock offset corresponding to the real-time clock offset is released. While generating the real-time clock offset, only the existing precise clock offset can be used to analyze the effect of the atomic clocks on it, but this may not be consistent with the state of the atomic clock that generated the real-time clock offset. Thinking in the opposite direction, we can roughly infer that the state of the atomic clock is defective when we do not find the exact reasons for the unsatisfactory results of the real-time clock offset estimation after analyzing various factors, and thus we can understand the atomic clock in advance.

6. Conclusions

This paper estimates the BDS real-time clock offset based on the MD model by using the observations of MGEX stations distributed in global/Asia-Pacific and evaluates the performance of the BDS atomic clocks. Then, two sets of clock offset are applied to kinematic PPP in different spatial scales, and the positioning performance of BDS is analyzed. The conclusions can be obtained from the research results of this paper as follows:

(1) The calculation accuracy of the BDS satellite clock offset estimated in Asia-Pacific is 0.102 ns, which can achieve a comparable accuracy of 0.093 ns with the globally estimated satellite clock offset. Regardless of the clock offset estimated in global or Asia-Pacific, the calculation accuracy of BDS-3 in all orbit types is better than BDS-2.

(2) In terms of the characteristics of BDS satellite atomic clocks, PHM clocks perform stabler than Rb clocks, and the BDS-2 atomic clocks are not as good as the BDS-3 due to aged hardware. In fact, several BDS-2 satellites have been in service for more than a decade, which explains why the estimated satellite clock corrections are unsatisfactory.

(3) The positioning accuracy of BDS-3 global kinematic PPP in the N, E and U directions can reach an average of 2.3, 3.6 and 5.9 cm, respectively, and the positioning accuracy of

the stations in the Asia-Pacific using the clock offset estimated in Global/Asia-Pacific is 1.9, 2.7, 4.9 cm and 2.2, 2.9, 5.2 cm in the N, E and U directions, respectively. This illustrates that BDS-3 can provide reliable and stable positioning results.

The BDS-3 satellite clock offset estimation model implemented in this research is real-time and fast calculation and can obtain high-precision clock offset, which can provide high-precision and all-weather positioning and navigation services in the Asia-Pacific and global.

Author Contributions: All authors made significant contributions to this study. Conceptualization, H.W. and P.L.; methodology, H.W. and P.L.; software, P.L.; validation, P.L.; formal analysis, P.L.; investigation, H.W.; writing—original draft preparation, P.L.; writing—review and editing, H.W., J.W., H.M., Y.H. and Y.R.; visualization, P.L.; funding acquisition, H.W. All authors have read and agreed to the published version of the manuscript.

Funding: This research is supported by the Key Project of China National Programs for Research and Development (No.2022YFB3903902; No.2022YFB3903900), the National Natural Science Foundation of China (No.42274044; No.41874042), and the Scientific Research Project of Chinese Academy of Surveying and Mapping (No.AR2101; No.AR2203; No.AR2214).

Data Availability Statement: The precise clock products were provided by the GFZ (https://gfz-potsdam.de/pub/GNSS/products, accessed on 23 October 2022).

Acknowledgments: The authors express great gratitude to GFZ for providing GNSS products. Additionally, the authors thank the GMT6 (Generic Mapping Tools) for making us convenient to plot some of the figures.

Conflicts of Interest: The authors declare that they have no conflict of interest.

References

1. Li, X.; Ge, M.; Dai, X.; Ren, X.; Fritsche, M.; Wickert, J.; Schuh, H. Accuracy and reliability of multi-GNSS real-time precise positioning: GPS, GLONASS, BeiDou, and Galileo. *J. Geod.* **2015**, *89*, 607–635. [CrossRef]
2. Bock, Y.; Melgar, D. Physical applications of GPS geodesy: A review. *Rep. Prog. Phys.* **2016**, *79*, 106801. [CrossRef] [PubMed]
3. Montenbruck, O.; Steigenberger, P.; Prange, L.; Deng, Z.; Zhao, Q.; Perosanz, F.; Romero, I.; Noll, C.; Sturze, A.; Weber, G.; et al. The Multi-GNSS Experiment (MGEX) of the International GNSS Service (IGS)—Achievements, prospects and challenges. *Adv. Space Res.* **2017**, *59*, 1671–1697. [CrossRef]
4. Yang, Y.; Gao, W.; Guo, S.; Mao, Y.; Yang, Y. Introduction to BeiDou-3 navigation satellite system. *Navigation* **2019**, *66*, 7–18. [CrossRef]
5. CSNO. BeiDou Navigation Satellite System Ground-based Augmentation Service Interface Control Document (Version 1.0). Available online: http://www.beidou.gov.cn/xt/gfxz/202008/P020200803362071652972.pdf (accessed on 23 October 2022).
6. Yang, Y.; Liu, L.; Li, J.; Yang, Y.; Zhang, T.; Mao, Y.; Sun, B.; Ren, X. Featured services and performance of BDS-3. *Chin. Sci. Bull.* **2021**, *66*, 2135–2143. [CrossRef]
7. Pan, J.; Hu, X.; Zhou, S.; Tang, C.; Guo, R.; Zhu, L.; Tang, G.; Hu, G. Time synchronization of new-generation BDS satellites using inter-satellite link measurements. *Adv. Space Res.* **2018**, *61*, 145–153. [CrossRef]
8. Ma, H.; Zhao, Q.; Verhagen, S.; Psychas, D.; Liu, X. Assessing the performance of multi-GNSS PPP-RTK in the local area. *Remote Sens.* **2020**, *12*, 3343. [CrossRef]
9. Shen, N.; Chen, L.; Lu, X.; Ruan, Y.; Hu, H.; Zhang, Z.; Wang, L.; Chen, R. Interactive multiple-model vertical vibration detection of structures based on high-frequency GNSS observations. *GPS Solut.* **2022**, *26*, 48. [CrossRef]
10. Ma, H.; Psychas, D.; Xing, X.; Zhao, Q.; Verhagen, S.; Liu, X. Influence of the inhomogeneous troposphere on GNSS positioning and integer ambiguity resolution. *Adv. Space Res.* **2021**, *67*, 1914–1928. [CrossRef]
11. Hauschild, A.; Montenbruck, O. Kalman-filter-based GPS clock estimation for near realtime positioning. *GPS Solut.* **2009**, *13*, 173–182. [CrossRef]
12. Zhang, X.; Li, X.; Guo, F. Satellite clock estimation at 1 Hz for realtime kinematic PPP applications. *GPS Solut.* **2011**, *15*, 315–324. [CrossRef]
13. Huang, G.; Qin, Z. Real-time estimation of satellite clock offset using adaptively robust Kalman filter with classified adaptive factors. *GPS Solut.* **2012**, *16*, 531–539. [CrossRef]
14. Chen, Y.; Yuan, Y.; Zhang, B.; Liu, T.; Ding, W.; Ai, Q. A modified mix-differenced approach for estimating multi-GNSS real-time satellite clock offsets. *GPS Solut.* **2018**, *22*, 72. [CrossRef]
15. Jaduszliwer, B.; Camparo, J. Past, present and future of atomic clocks for GNSS. *GPS Solut.* **2021**, *25*, 27. [CrossRef]
16. Fu, W.; Yang, Y.; Zhang, Q.; Huang, G. Real-time estimation of BDS/GPS high-rate satellite clock offsets using sequential least squares. *Adv. Space Res.* **2018**, *62*, 477–487. [CrossRef]

17. Kuang, K.; Wang, J.; Han, H. Real-time BDS-3 clock estimation with a multi-frequency uncombined model including new B1C/B2a signals. *Remote Sens.* **2022**, *14*, 966. [CrossRef]
18. Geng, T.; Jiang, R.; Lv, Y.; Xie, X. Analysis of BDS-3 onboard clocks based on GFZ precise clock products. *Remote Sens.* **2022**, *14*, 1389. [CrossRef]
19. Gu, S.; Mao, F.; Gong, X.; Lou, Y.; Xu, X.; Zhou, Y. Evaluation of BDS-2 and BDS-3 satellite atomic clock products and their effects on positioning. *Remote Sens.* **2021**, *13*, 5041. [CrossRef]
20. Ge, M.; Chen, J.; Douša, J.; Gendt, G.; Wickert, J. A computationally efficient approach for estimating high-rate satellite clock corrections in realtime. *GPS Solut.* **2012**, *16*, 9–17. [CrossRef]
21. Luzum, B.; Petit, G. The IERS Conventions (2010): Reference systems and new models. *Proc. Int. Astron. Union* **2012**, *10*, 227–228. [CrossRef]
22. Wu, J.; Wu, S.; Hajj, G.; Bertiger, W.; Lichten, S. Effects of antenna orientation on GPS carrier phase. *Manuscr. Geod.* **1993**, *18*, 91–98.
23. Schmid, R.; Dach, R.; Collilieux, X.; Jäggi, A.; Schmitz, M.; Dilssner, F. Absolute IGS antenna phase center model igs08. atx: Status and potential improvements. *J. Geod.* **2016**, *90*, 343–364. [CrossRef]
24. Dilssner, F.; Springer, T.; Schönemann, E.; Enderle, W. Estimation of satellite antenna phase center corrections for BeiDou. In Proceedings of the IGS Workshop 2014, Pasadena, CA, USA, 23–27 June 2014; pp. 23–27.
25. Bierman, G. *Factorization Methods for Discrete Sequential Estimation*; Academic Press Inc.: New York, NY, USA, 1977.
26. Saastamoinen, J. Contributions to the theory of atmospheric refraction. *Bull. Géodésique* **1972**, *105*, 279–298. [CrossRef]
27. Boehm, J.; Niell, A.; Tregoning, P.; Schuh, H. Global Mapping Function (GMF): A new empirical mapping function based on numerical weather model data. *Geophys. Res. Lett.* **2006**, *33*, L07304. [CrossRef]
28. CSNO-TARC. Fundamental PNT Service. Available online: http://www.csno-tarc.cn/en/system/constellation (accessed on 23 October 2022).
29. Zhang, W.; Lou, Y.; Gu, S.; Shi, C.; Haase, J.; Liu, J. Joint estimation of GPS/BDS real-time clocks and initial results. *GPS Solut.* **2016**, *20*, 665–676. [CrossRef]
30. Liu, T.; Zhang, B.; Yuan, Y.; Zha, J.; Zhao, C. An efficient undifferenced method for estimating multi-GNSS high-rate clock corrections with data streams in real time. *J. Geod.* **2019**, *93*, 1435–1456. [CrossRef]
31. Chen, J.; Zhao, X.; Hu, H.; Ya, S.; Zhu, S. Comparison and assessment of long-term performance of BDS-2/BDS-3 satellite atomic clocks. *Meas. Sci. Technol.* **2021**, *32*, 115021. [CrossRef]